Energy & Environmental Science

Cite this: *Energy Environ. Sci.*, 2012, **5**, 9543

www.rsc.org/ees

PAPER

Overall photocatalytic water splitting with NiO_x–$SrTiO_3$ – a revised mechanism

Troy K. Townsend,[a] Nigel D. Browning[ab] and Frank E. Osterloh*[a]

Received 26th June 2012, Accepted 20th August 2012
DOI: 10.1039/c2ee22665k

NiO_x ($0 < x < 1$) modified $SrTiO_3$ (STO) is one of the best studied photocatalysts for overall water splitting under UV light. The established mechanism for this and many other NiO_x containing catalysts assumes water oxidation to occur at the early transition metal oxide and water reduction at NiO_x. Here we show that NiO_x–STO is more likely a three component Ni–STO–NiO catalyst, in which STO absorbs the light, Ni reduces protons, and NiO oxidizes water. This interpretation is based on systematic H_2/O_2 evolution tests of appropriately varied catalyst compositions using oxidized, chemically and photochemically added nickel and NiO nanoparticle cocatalysts. Surface photovoltage (SPV) measurements reveal that Ni(0) serves as an electron trap (site for water reduction) and that NiO serves as a hole trap (site for water oxidation). Electrochemical measurements show that the overpotential for water oxidation correlates with the NiO content, whereas the water reduction overpotential depends on the Ni content. Photodeposition experiments with $NiCl_2$ and H_2PtCl_6 on NiO–STO show that electrons are available on the STO surface, not on the NiO particles. Based on photoelectrochemistry, both NiO and Ni particles suppress the Fermi level in STO, but the effect of this shift on catalytic activity is not clear. Overall, the results suggest a revised role of NiO in NiO_x–STO and in many other nickel-containing water splitting systems, including NiO_x–La : $KTaO_3$, and many layered perovskites.

Introduction

Splitting water into hydrogen and oxygen gas using suspended photocatalysts is generally considered the cheapest option for renewable hydrogen generation from sunlight.[1] However, photocatalysts that are capable of simultaneously reducing and oxidizing water are very rare.[2] Nickel oxide loaded strontium titanate ($SrTiO_3$, STO) is one of the few materials that can achieve the reaction in both pure water and aqueous NaOH solutions, without the need for expensive platinum group elements.[3–5] Consequentially, there has been interest in NiO_x–STO[3–6] and STO-based photocatalysts[7–12] for over three decades. Under UV irradiation, NiO_x–STO has been shown to photolyze water into H_2 (up to 100 μmol g^{-1} h^{-1}) and stoichiometric O_2.[13,14] Until today the accepted mechanism for NiO_x–STO,[5] and for many related photocatalysts,[15–17] including NiO_x–La : $KTaO_3$,[18] NiO_x–$K_4Nb_6O_{17}$ [19]

[a]*Department of Chemistry, University of California, Davis. One Shields Avenue, Davis, CA, 95616, USA. E-mail: fosterloh@ucdavis.edu; Fax: +1 530 752 8995*
[b]*Chemical and Materials Sciences Division, Pacific Northwest National Laboratory, 902 Battelle Boulevard P.O. Box 999, MSIN K8-87, Richland, WA 99352, USA*

Broader context

The water splitting reaction is generally regarded as the most promising method of converting solar energy into carbon free fuel. Among other catalysts, the reaction is promoted by NiO_x ($x = 0$–1)-modified $SrTiO_3$. This catalyst is particularly interesting because it does not require any rare elements to achieve its function. The accepted mechanism for water splitting with NiO_x–$SrTiO_3$ assumes that photogenerated electrons are transmitted to the Ni/NiO nanoparticles, which serve as proton reduction sites, whereas water oxidation occurs on the surface of $SrTiO_3$. Here we demonstrate an alternative mechanism, in which the NiO particles function as a water oxidation co-catalyst and the Ni particles as water reduction co-catalyst. This new interpretation is based on data from surface voltage spectroscopy, electrochemistry, photo-labeling and irradiation experiments. Thus, NiO_x–$SrTiO_3$ should be reformulated as a three-component catalyst Ni–$SrTiO_3$–NiO. The revised model resolves an old contradiction by Baba and Fujishima who stated in 1986 that 'NiO on $SrTiO_3$ powders was not the cathodic site for hydrogen evolution'. The model also has implications for other NiO_x containing photocatalysts, including NiO_x–La : $KTaO_3$, NiO_x–$K_4Nb_6O_{17}$ and NiO_x–$Rb_4Nb_6O_{17}$.

and NiO_x–$Rb_4Nb_6O_{17}$,[20] assumes that NiO_x functions as the proton reduction site, whereas water oxidation occurs at STO (or the layered metal oxide) using valence band holes. Based on high resolution electron microscopy data it has been shown that at least some of the NiO forms a shell around the Ni particles[5] which might function as a barrier for the reduction of oxygen, in analogy to the Cr_2O_3 shell in a related Rh–Cr_2O_3 system.[21,22] This established mechanism further assumes that STO acts as a photoanode, which is consistent with the n-type character of STO. Here we present experimental data that suggest that NiO_x–STO should instead be regarded as a three-component photocatalyst with a Ni water reducing cocatalyst and a separate NiO water oxidizing cocatalyst. This interpretation is supported by irradiation tests on Ni–STO–NiO photocatalysts with systematically varied composition, which demonstrate that the three components, STO, Ni, and NiO, are required for function. Furthermore, data from surface photovoltage (SPV) spectroscopy show that electron trapping occurs on Ni and hole trapping on NiO, and photolabeling experiments with platinum confirm that in NiO–STO, photoelectrons are predominantly located at STO and not at NiO. Finally, the assignments of Ni as a cocatalyst for proton reduction and that of NiO as a cocatalyst for water oxidation agree well with measurements of the electrochemical overpotentials of the catalysts. The reformulation of NiO_x–STO as a three-component system Ni–STO–NiO sheds a new light on this important photocatalyst and suggests new ways for optimizing its performance.

Results and discussion

Scheme 1 gives an overview of the preparation of materials relevant to this study. $SrTiO_3$ (STO) was prepared from a high temperature solid state synthesis from precursors.[23] Nickel and NiO were coupled to the STO *via* three complementary methods. Either capped nickel nanoparticles were co-precipitated with STO followed by reductive annealing to produce Ni(add)–STO or STO was irradiated in a Ni^{2+} solution to photodeposit nickel metal to generate Ni(*hv*)–STO. Or lastly, an aqueous solution of $Ni(NO_3)_2$ was deposited onto STO, followed by reductive annealing and re-oxidation at 130 °C to form *R*500–*O*130–NiO_x–STO and at 500 °C to form *R*500–*O*500–NiO–STO. In a subsequent step, the latter material was further modified by irradiating it in the presence of aqueous $NiCl_2$. This photodeposits nickel metal to produce Ni(*hv*)–*R*500–*O*500–NiO–STO.

The crystal structure and phase purity of STO were verified with powder XRD (Fig. 1). TEM images (Fig. 2A) of STO showed a particle size range of 100 nm–1 μm. Based on TEM and STEM images, *R*500–*O*130 NiO_x–STO was covered with both nickel metal and nickel oxide (Fig. 2B and inset) as revealed by a combination of dark and lighter (high Z-contrast) sites. Photodeposited NiO–STO showed small (4–6 nm) nickel particles distributed across STO (Fig. 2C and inset). In the case of Ni(add)–STO, 5–15 nm nickel nanoparticles can be seen to cover the surface of STO (Fig. 2D). Upon photodeposition of nickel onto *R*500–*O*500–NiO–STO, nickel particles (5–10 nm) are visible as dark Z-contrast particles (5–10 nm) in addition to larger NiO particles (25–50 nm) from the initial oxidation process (Fig. 2E). Pt(*hv*)–*R*500–*O*500–NiO–STO (Fig. 2F) shows discrete photolabeled Pt particles (0.5–1.0 nm) on the STO surface in addition to separated NiO particles (5–10 nm). Similar to the Ni particles in Ni(*hv*)–NiO–STO, the Pt particles appear to be spatially isolated from the NiO sites.

UV/Vis diffuse reflectance spectra of unmodified STO (white powder, Fig. 3A) and NiO-activated STO catalysts (grey powders) show optical absorption onset between 3.0 and 3.2 eV, in agreement with the reported indirect band gap of 3.20 eV (O 2p → Ti 3d t_{2g}/e_g).[24]

Only small changes occur upon addition of Ni nanoparticles, which is mostly a result of the low Ni content (3% mass) in the samples and the small Ni particle sizes (<5 nm in Ni(*hv*)–STO and <15 nm in Ni(add)–STO). In contrast, both *R*500–*O*25–Ni–STO and *R*500–*O*130–NiO–STO show a broad sub-band gap absorption with a peak at around 2.6 eV. Similar optical features have been previously attributed to $SrTiO_3$ doping with transition metal ions, including Ni^{2+} and Fe^{2+}.[25,26]

Surface photovoltage (SPV) spectroscopy is a useful tool for the characterization of photo-induced charge transfer processes in inorganic semiconductors and photocatalysts.[27–31] In SPV a light-induced change of the contact potential difference (ΔCPD *versus* gold) of a sample is recorded as a function of the irradiation wavelength/energy. This produces positive or negative photovoltages, depending on the direction of charge transport. Spectra for thin films of STO and nickel derivatives are shown in Fig. 3B. Unmodified STO only produces a small ΔCPD signal of −70 mV, at photon energies of 3.40 eV, above the optical band gap of the material. The negative sign signifies that electrons are separated towards the gold substrate and that holes accumulate on the surface of the material. When the STO particles are coated

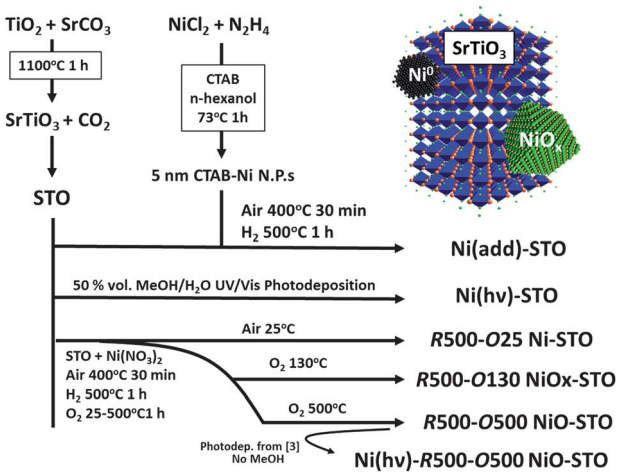

Scheme 1 Synthesis of STO and NiO and Ni derivatives.

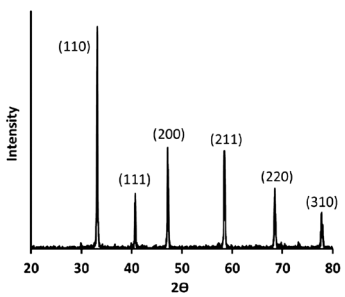

Fig. 1 Powder X-ray diffraction pattern of synthesized STO.

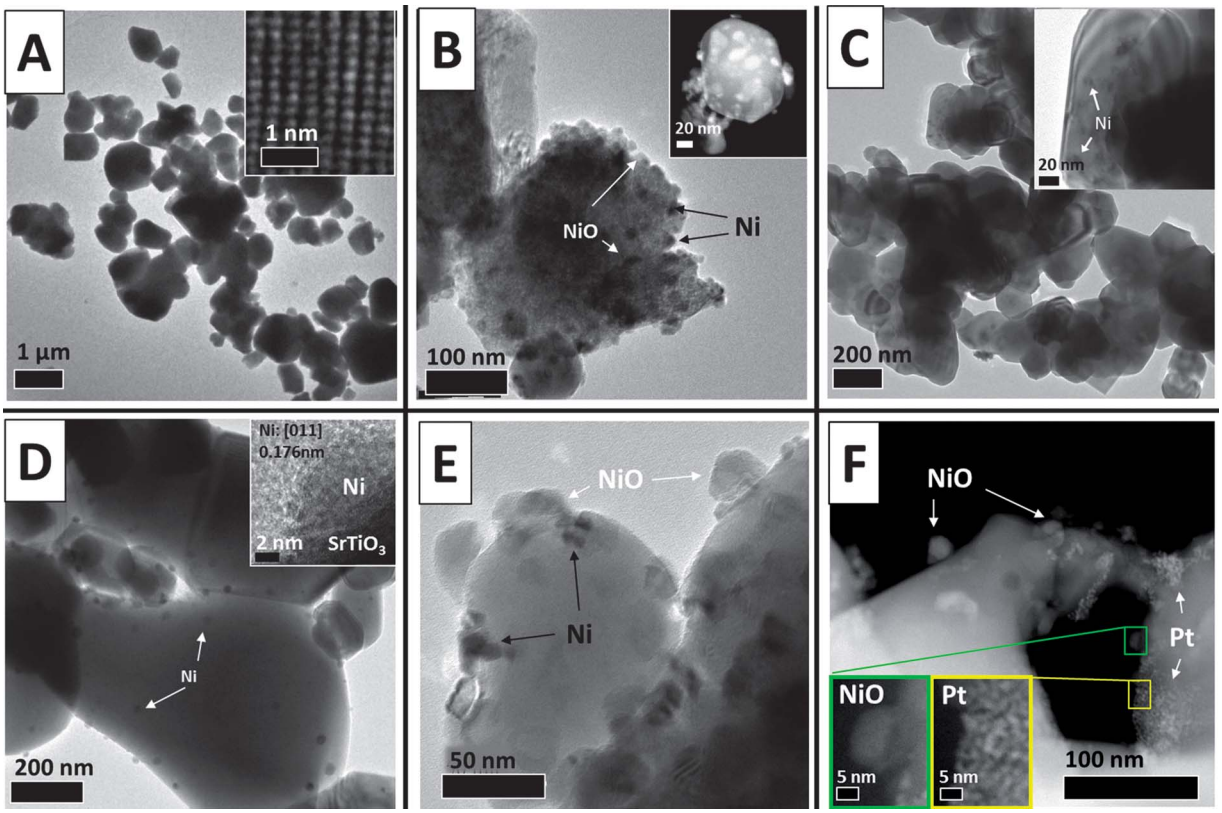

Fig. 2 TEM of STO [A], TEM and HRSTEM of *R*500–*O*130–NiO_x–STO [B], HRTEM of Ni(*hν*)–STO [C], Ni(add)–STO [D], Ni(*hν*)–*R*500–*O*500–NiO–STO [E] and HRSTEM of Pt(*hν*)–*R*500–*O*500–NiO–STO [F].

with NiO_x as in *R*500–*O*130–NiO_x–STO, the negative ΔCPD signal increases and reaches a value of −460 mV at 3.68 eV. The enhancement of the positive polarization of the sample suggests that NiO_x serves as a hole-trapping material. In contrast, Ni(add)–STO yields a positive ΔCPD trace suggestive of electron trapping on the sample. The maximum value of this signal (+370 mV) is reached at 3.80 eV, at similar photon energy as in the preceding spectra. A positive ΔCPD signal is also observed for Ni(*hν*)–STO, but here the maximum ΔCPD value (+220 mV) is slightly smaller. Both of these materials predominantly contain Ni(0) and only a small fraction of NiO (from sporadic exposure to air at 25 °C). Therefore, we conclude that Ni(0) acts as an electron trap on the STO. This interpretation agrees well with the concept of photochemical diodes where metal particles on photocatalysts act as electron acceptors and with the use of Ni(0) as a catalyst for the hydrogen evolution reaction.[11,32–34]

To specifically probe the effect of the NiO/Ni ratio in *R*500–*O*25 Ni–STO on charge separation, the compound was subjected to controlled oxidation by heating in air from 25 °C → 50 °C → 100 °C → 130 °C → 500 °C, followed by cooling to 25 °C. In this series, subsequent calcination steps convert an increasing amount of the nickel metal into NiO. The corresponding SPV spectra for the series are shown in Fig. 4A. While the first two samples yield positive SPV signals indicating electron trapping in the film, the latter samples show negative SPV spectra, with increasing size of the CPD value. This further confirms the interpretation of nickel metal particles acting as electron traps whereas NiO particles serve as hole traps. The proposed mechanism of charge separation in the three systems is also shown schematically in Fig. 4B. When both Ni metal and NiO are present, the effects of electron and hole trapping compensate each other. This situation is most closely realized in the *R*500–*O*50 Ni–STO sample.

The chemical transformation of Ni(0) into NiO is also reflected in the morphologies of the materials. While most of the cocatalyst particles in *R*500–*O*25 Ni–STO are pure nickel (based on contrast), some show evidence of a less dense shell that is presumably made of NiO (inset of Fig. 4C), as has been previously observed by Domen and coworkers.[5] The more strongly oxidized sample *R*500–*O*130 NiO_x–STO shows a combination of high Z-contrast Ni particles and low Z-contrast NiO particles (Fig. 4D), and lastly, *R*500–*O*500 NiO–STO displays only large (50–100 nm) NiO particles of low contrast (Fig. 4E), in agreement with full Ni oxidation at the higher oxidation temperature.

In order to verify the proposed charge separation scheme in Fig. 4B, a photo-labelling experiment was performed with *R*500–*O*500–NiO–STO. The material was dispersed in pure water and irradiated in the presence of H_2PtCl_6 (no methanol was added to avoid reduction of NiO). Under these conditions Pt^{4+} gets quickly reduced to Pt(0) by photoelectrons generated in STO. A HRSTEM image of the irradiated material is shown in Fig. 5A. Small Pt particles (0.1–1 nm) can be found on the surface of the STO particles, clearly separated from the larger (5–10 nm) NiO particles (Fig. 2F and 5A). The identity of the particles is confirmed by repeated EDS line scans on the Ni (K,L) and Pt (L) emission lines (Fig. 5B). The fact that Pt(IV) is reductively photodeposited onto the STO surface and not onto the NiO particles supports the role of NiO as a hole acceptor in the NiO–STO system, as proposed in Fig. 4B.

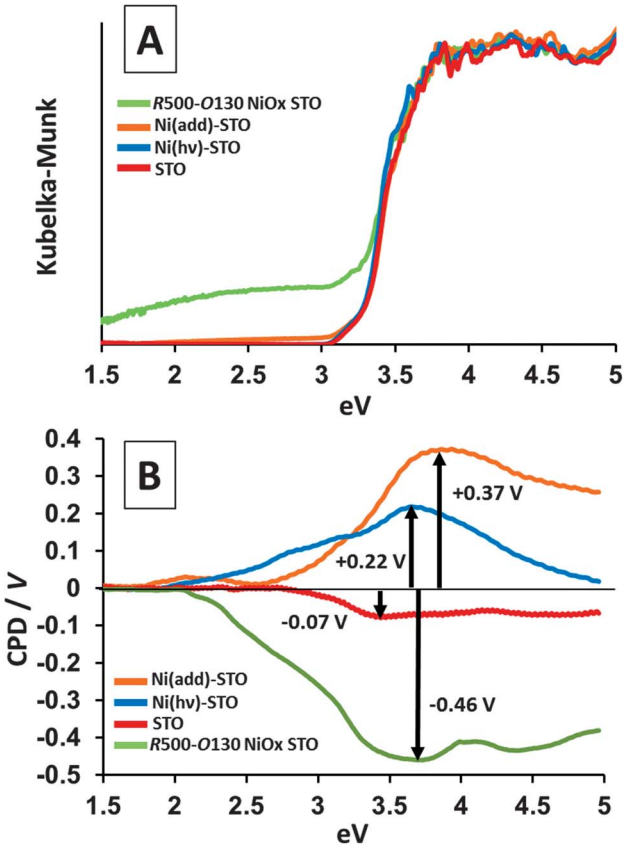

Fig. 3 (A) UV/Vis diffuse reflectance spectra (Kubelka Munk) of STO and NiO_x–STO. (B) Surface photovoltage spectra of STO samples on a gold electrode under vacuum (2×10^{-4} mbar); the max. excitation power is 0.8 mW cm^{-2}. To correct for sample drift, each shown spectrum is the difference between a light scan and a scan in the dark.

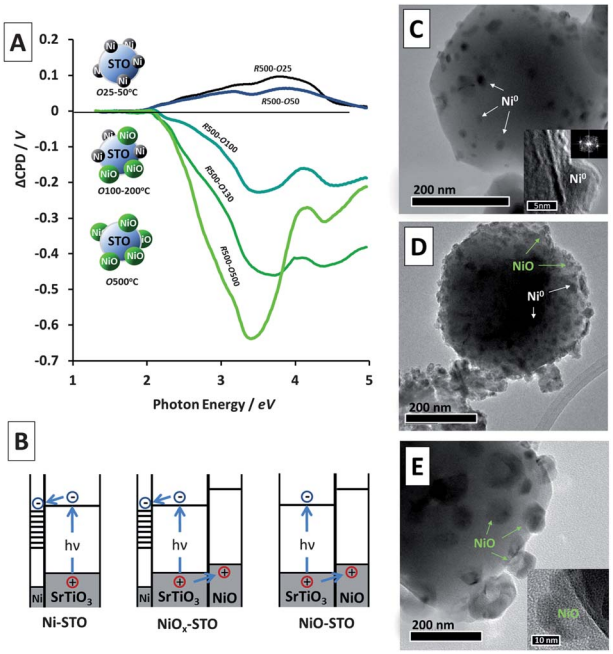

Fig. 4 [A] Light-induced contact potential change (ΔCPD) of 3 wt% NiO–STO films on a gold glass electrode under vacuum (2×10^{-4} mbar) *versus* excitation energy. Materials after reduction at 500 °C followed by re-oxidation at 25 °C (black), 50 °C (blue), 100 °C (cyan), 130 °C (dark green), and 500 °C (light green). [B] Proposed electron–hole separation at STO–Ni and STO–NiO interfaces. HRTEM images of *R*500–*O*25–Ni–STO [C], *R*500–*O*130–NiO_x–STO [D], and *R*500–*O*500–NiO–STO [E].

In order to gain further insight into the roles of Ni and NiO, catalyst powders were dispersed in pure water under inert atmosphere and irradiated with a 300 W Xe arc lamp ($\lambda >$ 250 nm). As the most active catalyst, *R*500–*O*130–NiO_x–STO was found to evolve stoichiometric amounts of H_2 and O_2 over the entire 24 h time interval with the activity slightly diminishing after the first 5 h to a final 28 μmol g^{-1} h^{-1} (Fig. 6A). This activity is about 30% of the value for bulk NiO_x–$SrTiO_3$ (100 μmol g^{-1} h^{-1}) reported by Domen in 1982.[14] Slightly lower activity (22.5 μmol g^{-1} h^{-1}, Fig. 6B) and sub-stoichiometric O_2 evolution were observed for Ni(*hv*)–STO, indicating that water oxidation was a limiting factor in this catalyst.

Interestingly, *R*500–*O*500–NiO–STO was not active at all (Fig. 6C), possibly owing to the lack of nickel metal in this material. To verify this hypothesis, nickel nanoparticles were photodeposited onto the inactive *R*500–*O*500–NiO–STO to obtain Ni(*hv*)–*R*500–*O*500–NiO–STO. This did activate the material for stoichiometric H_2/O_2 evolution at a rate of 6.86 μmol g^{-1} h^{-1}, as shown in Fig. 6C. Finally, Ni(add)–STO was also found to be active for stoichiometric H_2/O_2 evolution, although at low rates (5.3 μmol g^{-1} h^{-1}, Fig. 6D). In order to determine to what extent this catalyst was limited by the low content of NiO, the material was calcined in O_2 at 130 °C for 1 h. This treatment did increase the activity of the catalyst by 27% (Fig. 6D), signifying the importance of NiO in the catalysts. Overall, the irradiation experiments showed that the presence of both nickel metal and NiO is required for efficient stoichiometric H_2/O_2 evolution.

To further probe the involvement of Ni and NiO in the water splitting process, electrochemical scans were conducted on films of the catalysts on gold electrodes immersed in phosphate-buffered water at pH = 7. Potential current curves are shown in Fig. 7 and calculated overpotentials are listed in Table 1. Water reduction is found to occur at potentials negative of −0.50 V for all catalysts. Unmodified STO and pure NiO have the largest overpotentials for proton reduction (η = 0.44 V and 0.47 V, respectively). The attachment of Ni particles to STO reduces the overpotential to 0.39 V for Ni(*hv*)–STO and to 0.36 V for Ni(add)–STO. The catalyst containing both NiO and Ni (*R*500–*O*130 NiO_x–STO) has η = −0.35 V, *i.e.* +0.09 V better than unmodified STO. This clearly shows that the Ni(0) metal promotes water reduction in these catalysts.

Anodic scans to probe the water oxidation potentials are shown in Fig. 7B. Water oxidation takes place at potentials between +1.2 V and +1.6 V, depending on the sample, and is accompanied by gas bubble formation at the electrode. Plain NiO (η = 0.61 V) was found to oxidize water most easily, followed by *R*500–*O*130 NiO_x–STO (η = 0.71 V). Overpotentials for the remaining samples increase in order Ni(*hv*)–STO (+0.77 V) < Ni(add)–STO (+0.78 V) < STO (+0.80 V). As the latter samples contain the smallest fraction of NiO, the relative order shows clearly that the ease of electrochemical water oxidation is correlated with the NiO content in each catalyst. In

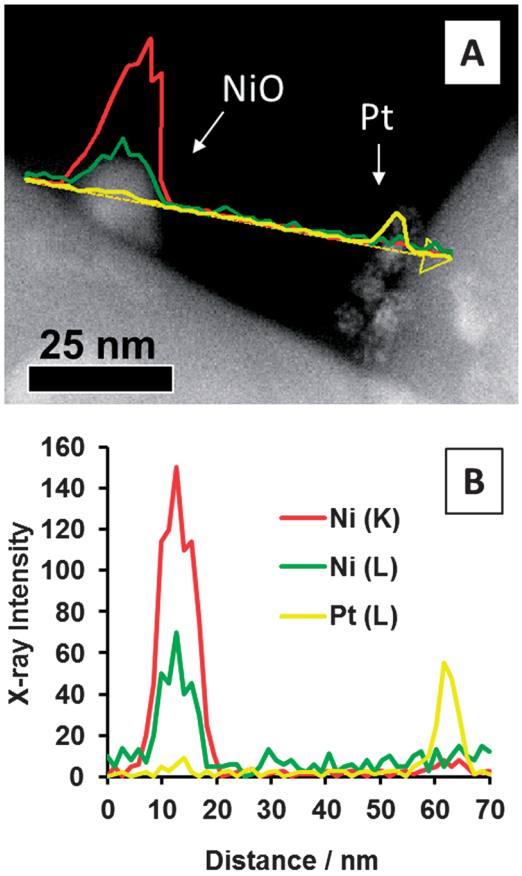

Fig. 5 [A] HRSTEM image of Pt(*hv*)–*R*500–*O*500–NiO–STO and [B] EDS line scan.

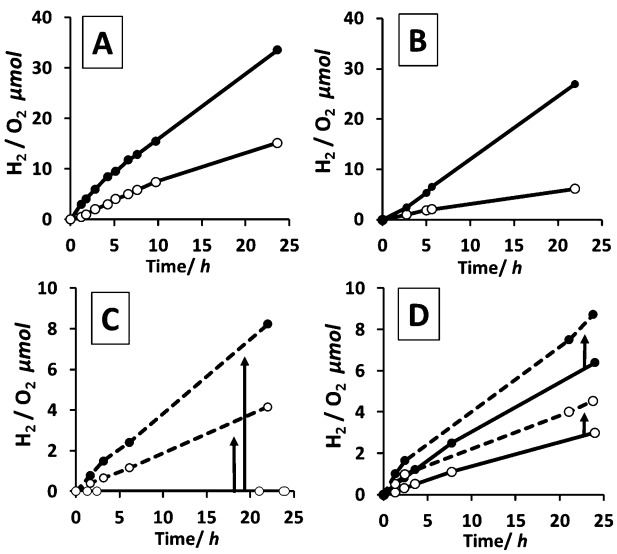

Fig. 6 H_2 and O_2 evolution from 272 µmol (50 mg) NiO_x loaded STO suspended in 50 mL of water at pH 7 under full spectrum irradiation (>250 nm). [A] *R*500–*O*130–NiO_x–STO, [B] Ni(*hv*)–STO, [C] inactive *R*500–*O*500–NiO–STO (solid line) and activated Ni(*hv*)–*R*500–*O*500–NiO–STO (dashed line), [D] Ni(add)–STO–*R*500–*O*25 (solid line) and Ni(add)–STO–*R*500–*O*130 (dashed line).

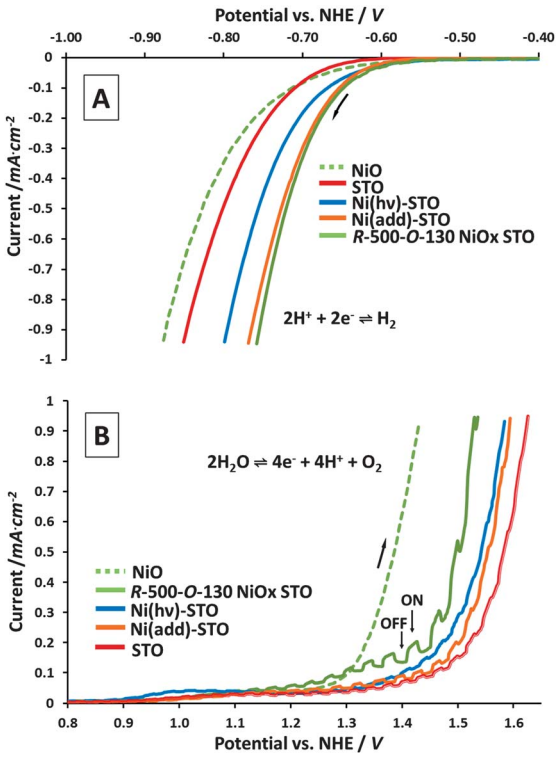

Fig. 7 Photo-electrochemical water reduction [A] and oxidation [B] with NiO_x–STO films on the Au substrate, 10 mV s^{-1} scans, at pH = 7 in Na_2HPO_4–NaH_2PO_4 buffer. All potentials are referenced against NHE.

contrast, proton reduction is limited by the Ni metal content. These assignments also agree well with the literature. Nickel metal is widely known as an electrocatalyst for the HER reaction[34–36] and NiO is an electrocatalyst for the oxygen evolution reaction (OER).[37] The analysis also shows that η_{OX} values are about twice as large as the η_{Red} values. Thus the overall performance of the catalysts appears limited by the water oxidation kinetics. Indeed, it is well known that the best activity of NiO_x–STO can be achieved in alkaline solution, where water oxidation is thermodynamically more favorable.[38]

Lastly, in order to observe the effect of Ni/NiO modification on the energetics of STO, photoelectrochemical scans were also performed on films of the catalysts on gold foil, immersed into 0.1 M aqueous KCl (pH 7) with 10% (vol) added methanol. The photo-onset potential E_{Ph} recorded under these conditions signifies the quasi Fermi level of the electrons in $SrTiO_3$.[39,40] For heavily n-doped materials, this value is close to the conduction

Table 1 Electrochemical and photoelectrochemical data. Water reduction and oxidation overpotentials (η, at 0.90 mA cm^{-2}) are referenced against the thermodynamic potentials at pH 7 (−0.413 V NHE H^+/H_2 and +0.817 V NHE O_2/H_2O)

Catalyst	E_{Ph}/ V *vs.* NHE	η_{Red}/ V	η_{Ox}/ V	H_2 rate/ µmol g^{-1} h^{-1}
Bulk STO	−0.87	0.44	0.80	0.00
Ni(add)–STO	−0.67	0.36	0.78	5.33
Ni(*hv*)–STO	—	0.39	0.77	22.5
*R*500–*O*130–NiO_x–STO	−0.40	0.35	0.71	28.0

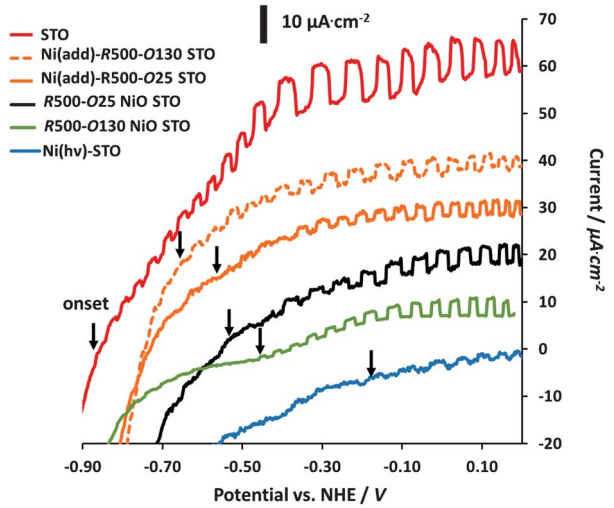

Fig. 8 Photo-current scans of NiO_x–STO films on the Au substrate, 10 mV s^{-1} scan rate, at pH = 7 in aqueous 0.1 M KCl containing 10 vol% methanol. Arrows mark values for E_{Ph}.

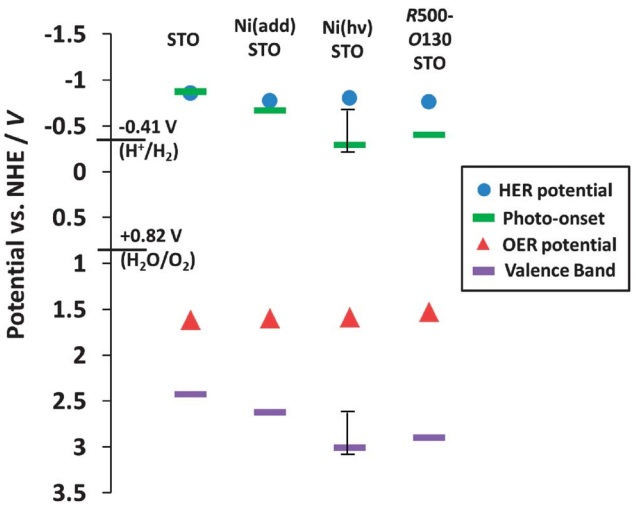

Fig. 9 Energy diagram of catalysts in order of increasing activity (left to right). The trend in water redox potentials is obscured by the energy scale of the scheme. The reader is referred to Fig. 7 instead.

band edge of the semiconductor. The electrochemical scans are shown in Fig. 8 and relevant data collected in Table 1. Observed photocurrents were 20 μA cm^{-2} for STO but decreased to ~3 μA cm^{-2} upon attachment of Ni/NiO. In the case of Ni(*hv*)–STO, photocurrents were too small to accurately determine the photoonset. The photocurrent decrease is due to competitive light absorption by NiO and Ni particles in the UV region of the spectrum, increased electron hole recombination at the Ni–STO and STO–NiO interfaces and electron trapping at Ni particles.

For unmodified STO we obtain $E_{Ph} = -0.87$ V, in excellent agreement with the pH-corrected value of −0.89 V, NHE for the flatband potential of $SrTiO_3$ (Butler and Ginley, −0.95 V at pH 8.6).[41] Upon attachment of NiO or Ni particles, the photo-onset potential shifts to values between −0.67 and −0.41 V. Similar changes of E_{Ph} were observed for niobate and titanate nanocrystals upon addition of platinum or IrO_x nanoparticles.[42,43] Because the Fermi energies of Ni, Pt, IrO_x, and NiO are more positive than $SrTiO_3$, the electrochemical equilibrium causes electrons to move from $SrTiO_3$ to the cocatalyst.

The energetics of the photocatalysts are summarized in Fig. 9, in order of increasing photocatalytic activity (left to right). The $SrTiO_3$ conduction band edges were approximated with E_{Ph} values from Table 1 (the true conduction band edges are at more negative potentials). The following trends can be observed in the diagram (in order of increasing activity). (1) The $SrTiO_3$ band edges become more positive. (2) The HER potential becomes more positive (proton reduction gets easier). (3) The OER potential becomes less positive (water oxidation gets easier).

Thus optimized performance is the result of the combination of a low proton reduction overpotential with a low water oxidation overpotential, as discussed above. This can be achieved by having both Ni and NiO cocatalysts present at the same time. The positive shift of the $SrTiO_3$ band edges from left to right is an indirect result of the loading with cocatalysts. Theoretically, this shift should also promote the water oxidation reaction and slow the water reduction reaction. But the significance of this effect cannot be established in the presence of the other parameters.

Conclusion

Overall, the findings presented here suggest that the Ni/NiO cocatalyst in the known NiO_x–STO system may not just be involved in proton reduction but also in water oxidation. The interpretation of NiO_x–STO as a three component system with a STO light absorber, a Ni proton reduction and a NiO water oxidation catalyst is supported by the following observations. (1) Both Ni metal and NiO are required as cocatalysts on $SrTiO_3$ for photocatalytic water splitting. (2) Non-active NiO–STO can be activated for water splitting by photodeposition of Ni metal. (3) Based on surface photovoltage spectroscopy, Ni acts as an electron trap and NiO as a hole trap. (4) Reductive photodeposition of Pt occurs on $SrTiO_3$, not on NiO, tracing photogenerated electrons in that material. (5) Based on electrochemistry, Ni(0) lowers the proton reduction overpotential, while NiO lowers the water oxidation overpotential. Additional photoelectrochemical data show that both Ni and NiO shift the photoonset potential (a measure of the $SrTiO_3$ conduction band edge) to more positive values, but it is not clear if this shift is significant for activity. The reinterpretation of NiO as the water oxidation site might be relevant to other NiO_x-derived water splitting catalysts,[15,16,19] including NiO_x–La : K-TaO_3,[18] NiO_x–$K_4Nb_6O_{17}$,[19] and NiO_x–$Rb_4Nb_6O_{17}$.[20] Similar to NiO_x–STO, those catalysts also require partial re-oxidation of the Ni-component to reach optimal activity. The new findings also resolve an early contradiction by Baba and Fujishima in 1986, who conclude that 'on the basis of the hydrogen separation factor analysis for NiO–$SrTiO_3$, it seemed that the surface of the deposited NiO on $SrTiO_3$ powders was not the cathodic site for hydrogen evolution'.[44] Lastly, this work also shows that the performance of the Ni–STO–NiO system is limited by the electrochemical overpotential for water oxidation, which is twice as high as that for water reduction. Thus, an increase of the activity should be possible by replacing NiO with a more effective water oxidation catalyst. Or alternatively, alkaline conditions can be employed to promote water oxidation.[12,38]

Experimental

Chemicals KOH 99.9%, oxalic acid 99.9%, $Sr(NO_3)_2$ 99.9%, P25 TiO_2, $Ni(H_2O)_6(NO_3)_2$ 99.9%, $NiCl_2 \cdot 6H_2O$ 99.9%, cetyltrimethylammonium bromide, CTAB, 99.9%, and *n*-hexanol 99.9% were purchased from Fisher Scientific, Pittsburgh, PA. Water was purified to 18 MΩ cm resistivity using a Nano-pure system.

STO particles

STO was synthesized *via* a high temperature solid state process[23] where 0.02 mol, 1.74 g P25 TiO_2 was mixed and sonicated for 10 minutes with 0.026 mol, 5.53 g $Sr(NO_3)_2$ in a 1 : 1.2 molar ratio in 200 mL of water to produce precursors for 4 g of $SrTiO_3$. Aqueous oxalic acid (0.4 M, 1 : 1 molar ratio with Sr) was added drop wise to the solution under vigorous stirring. Conc. ammonium hydroxide was added slowly to increase the pH of the solution to 6.5 in order to precipitate strontium oxalate crystals onto the 25 nm TiO_2 particle surfaces *via* heterogeneous nucleation.[45] When precipitation was complete, the white solid was centrifuged and washed 8 times in 50 mL of water, followed by drying in air at 100 °C. This precursor was calcined in a Thermolyne 79300 Tube Furnace to 1100 °C for 1 h with a heating rate of 10 °C min^{-1}. After cooling down to room temperature, the white solid was washed twice in 50 mL of 5 M HNO_3 to remove excess $SrCO_3$ followed by repeated water washes until the supernatant reached a pH of 7. Phase purity was confirmed by powder X-ray diffraction.

Modification with $Ni(NO_3)_2$

STO particles (200 mg, 1.10 mmol) were added to a 20 mL aqueous $Ni(NO_3) \cdot 6H_2O$ solution (0.023 g, 3 wt% loading of NiO : STO), and the components were thoroughly mixed in a sonication bath for 10 min. This solution was dried at 100 °C and then annealed at 400 °C in air for 30 min to produce a grey colored solid. The solid was then heated in an H_2 atmosphere to 500 °C and maintained at that temperature for 1.5 h to remove nitrate as $N_{2(g)}$ and $H_2O_{(l)}$ and to simultaneously reduce Ni^{2+} to Ni(0). After that, the black solid was heated in an O_2 atmosphere at 25 °C, 50 °C, 100 °C, 130 °C, or 500 °C for 30 min to induce oxidation of nickel to nickel oxide (NiO_x, $0 < x < 1$).[5]

Modification with nickel(I)

STO particles (50 mg, 2.7×10^{-4} mol) were suspended in 50 mL of aqueous methanol (1 : 1 v/v) containing 0.013 M (0.195 g) of $NiCl_2 \cdot 6H_2O$. This mixture was irradiated using a xenon arc lamp for 24 h until the solution changed from white to dark grey.[46] The resulting grey solid was centrifuged and washed 4 times with 50 mL of water followed by drying at room temperature.

Modification with nickel or platinum(II)

Fully oxidized *R*500–*O*500–NiO–STO particles were prepared as described above by calcination at 500 °C. The solid was then dispersed in aqueous $NiCl_2 \cdot 6H_2O$ (0.013 M) solution and irradiated with a Xe arc lamp for 24 h. The product was obtained by centrifugation and washed four times in 50 mL of H_2O. No methanol was used in the preparation because irradiation in methanol can cause (back-) conversion of NiO to Ni. For the preparation of Pt(*hv*)–*R*500–*O*500–NiO–STO, H_2PtCl_6 (1.0 wt% Pt) was used in place of $NiCl_2 \cdot 6H_2O$.

Modification with nickel(III)

Nickel nanoparticles (5–10 nm) were synthesized following a literature method.[47] Two separate microemulsions ($NiCl_2$ [0.1 M]/CTAB/*n*-hexanol and N_4H_5OH [3 M]/CTAB/*n*-hexanol, adjusted to pH 13 with conc. ammonia) were mixed giving a final wt% ratio = 22% H_2O : 33% CTAB : 45% *n*-hexanol. This solution was heated and stirred at 73 °C for 1 h to produce 5–10 nm Ni nanoparticles. STO particles (200 mg, 1.10 mmol) were added to 20 mL of this dispersion. The dispersion was mixed in a sonication bath for 10 min and the STO and Ni NPs were co-precipitated by adding 100 mL of methanol : chloroform (1 : 1 vol). The resulting solid was washed four times with 50 mL of H_2O and dried at 100 °C, in air. After an additional treatment in air (400 °C for 1 h) and H_2 (500 °C for 1 h), the sample was cooled down to 25 °C and handled in air.

Preparation of plain NiO

$Ni(NO_3)_2 \cdot 6H_2O$ was heated in air at 400 °C for 1 h, followed by H_2 atmosphere (500 °C for 1 h) and then O_2 (500 °C for 1 h) to form a dark green solid and phase verified with XRD (data not shown).

Powder XRD scans were conducted with a Scintag XRD, at a wavelength of $\lambda = 0.154$ nm with 2 mm tube slit divergence, 4 mm scatter, 0.5 mm column scatter and 0.2 mm receiving widths.

Bright field high resolution transmission electron microscopy (HRTEM) and HR scanning transmission electron microscopy (HRSTEM) images were taken using a JEOL 2500SE 200 kV T/STEM. Energy Dispersive X-ray Spectroscopy (EDS) scans were taken in STEM mode with a ThermoNORAN Spectrophotometer and NORAN System SIX analysis program. Samples were prepared by immersing copper grids with a carbon film into aqueous dispersions of the samples followed by washing with water and air-drying.

UV/Vis diffuse reflectance spectra were recorded on dried powders on white Teflon tape using a Thermo Scientific Evolution 220 UV Vis spectrometer eqipped with an integrating sphere.

For electrochemical measurements, thin films of the catalysts were prepared on a gold foil electrode (1.0 cm^2) by drop coating and drying at 25 °C. A wire was attached to the bare gold back with conductive carbon tape and sealed with adhesive. The electrode was placed into a N_2-purged 3-electrode cell with a Pt counter electrode and a saturated calomel reference electrode connected to the cell with a KCl salt bridge. The cell was filled to 50 mL with 0.25 M Na_2HPO_4–NaH_2PO_4 buffer solution at pH 7, and the solution was degassed with N_2. Dark cyclic voltammetry scans were taken at 50 mV s^{-1}. The system was calibrated using the redox potential of $K_4[Fe(CN)_6]$ at +0.358 V (NHE). For light measurements, 5 mL methanol was added to the solution, and chopped light was introduced into the cell using a fiber optics cable connected to a 300 W Xe arc lamp.

Surface photovoltage (SPV) measurements were conducted under vacuum (2×10^{-4} mBar) on $SrTiO_3$ films on gold

substrates. A gold Kelvin probe (Delta PHI Besocke) served as the reference electrode. Samples were illuminated with monochromatic light from a 150 W Xe lamp filtered through an Oriel Cornerstone 130 monochromator (1–10 mW cm^{-2}). The CPD spectra were corrected for drift effects by subtracting a dark scan. The rate of photochemical hydrogen and oxygen evolution from each catalyst was determined by irradiating 50 mg (~0.27 mmol) of photocatalyst dispersed in 50 mL of Nano-pure water.

Irradiations were performed in a quartz round bottom flask using light from a 300 W Xe arc lamp (26.3 mW cm^{-2} at the flask λ = 250–380 nm, measured with a GaN photodetector), after filtering out the infrared portion with a water filter. The air-tight irradiation system connects a vacuum pump and a gas chromatograph (Varian 3800) with the sample flask to quantify the amount of gas evolved, using area counts of the recorded peaks. Prior to irradiation, the flask was evacuated down to 5 Torr and purged with argon gas. This cycle was repeated until the chromatogram of the atmosphere above the solution indicated that the sample did not contain hydrogen, oxygen, or nitrogen.

Acknowledgements

FEO thanks Research Corporation for Science Advancement for a Scialog award. This work was further supported by the National Science Foundation (NSF, grant number 1133099) and by the US Department of Energy under grant number FG02-03ER46057. TKT thanks NSF for a Graduate Research Fellowship 2012.

References

1 B. D. James, G. N. Baum, J. Perez and K. N. Baum, Technoeconomic Analysis of Photoelectrochemical (PEC) Hydrogen Production, DOE Contract Number: GS-10F-009J DOE Technical Monitor: David Peterson, 2009, **1**, 1–128, Web: http://www1.eere.energy.gov/hydrogenandfuelcells/pdfs/pec_technoeconomic_analysis.pdf.
2 F. E. Osterloh, *Chem. Mater.*, 2008, **20**, 35–54.
3 K. Domen, S. Naito, M. Soma, T. Onishi and K. Tamaru, *J. Chem. Soc., Chem. Commun.*, 1980, **12**, 543–544.
4 K. Domen, S. Naito, T. Onishi and K. Tamaru, *J. Phys. Chem.*, 1982, **86**, 3657–3661.
5 K. Domen, A. Kudo and T. Onishi, *J. Catal.*, 1986, **102**, 92–98.
6 R. Niishiro, H. Kato and A. Kudo, *Phys. Chem. Chem. Phys.*, 2005, **7**, 2241–2245.
7 J. W. Liu, G. Chen, Z. H. Li and Z. G. Zhang, *J. Solid State Chem.*, 2006, **179**, 3704–3708.
8 Y. Sasaki, A. Iwase, H. Kato and A. Kudo, *J. Catal.*, 2008, **259**, 133–137.
9 Y. Sasaki, H. Nemoto, K. Saito and A. Kudo, *J. Phys. Chem. C*, 2009, **113**, 17536–17542.
10 K. Iwashina and A. Kudo, *J. Am. Chem. Soc.*, 2011, **133**, 13272–13275.
11 J. M. Lehn, J. P. Sauvage and R. Ziessel, *New J. Chem.*, 1980, **4**, 623–627.
12 S. X. Ouyang, H. Tong, N. Umezawa, J. Y. Cao, P. Li, Y. P. Bi, Y. J. Zhang and J. H. Ye, *J. Am. Chem. Soc.*, 2012, **134**, 1974–1977.
13 K. Sayama and H. Arakawa, *J. Photochem. Photobiol., A*, 1994, **77**, 243–247.
14 K. Domen, S. Naito, T. Onishi and K. Tamaru, *Chem. Phys. Lett.*, 1982, **92**, 433–434.
15 T. Takata, Y. Furumi, K. Shinohara, A. Tanaka, M. Hara, J. N. Kondo and K. Domen, *Chem. Mater.*, 1997, **9**, 1063–1064.
16 S. Ikeda, M. Hara, J. N. Kondo, K. Domen, H. Takahashi, T. Okubo and M. Kakihana, *Chem. Mater.*, 1998, **10**, 72–77.
17 A. Kudo and Y. Miseki, *Chem. Soc. Rev.*, 2009, **38**, 253–278.
18 H. Kato, K. Asakura and A. Kudo, *J. Am. Chem. Soc.*, 2003, **125**, 3082–3089.
19 A. Kudo, K. Sayama, A. Tanaka, K. Asakura, K. Domen, K. Maruya and T. Onishi, *J. Catal.*, 1989, **120**, 337–352.
20 K. Sayama, A. Tanaka, K. Domen, K. Maruya and T. Onishi, *J. Catal.*, 1990, **124**, 541–547.
21 K. Maeda, A. K. Xiong, T. Yoshinaga, T. Ikeda, N. Sakamoto, T. Hisatomi, M. Takashima, D. L. Lu, M. Kanehara, T. Setoyama, T. Teranishi and K. Domen, *Angew. Chem., Int. Ed.*, 2010, **49**, 4096–4099.
22 K. Maeda, K. Teramura, D. L. Lu, N. Saito, Y. Inoue and K. Domen, *J. Phys. Chem. C*, 2007, **111**, 7554–7560.
23 P. K. Roy and J. Bera, *Mater. Res. Bull.*, 2005, **40**, 599–604.
24 K. v. Benthem, C. Elsasser and R. H. French, *J. Appl. Phys.*, 2001, **90**, 6156–6164.
25 R. L. Wild, E. M. Rockar and J. C. Smith, *Phys. Rev. B: Solid State*, 1973, **8**, 3828–3835.
26 B. Jalan, R. Engel-Herbert, T. E. Mates and S. Stemmer, *Appl. Phys. Lett.*, 2008, **93**, 1365–1367.
27 L. Kronik and Y. Shapira, *Surf. Sci. Rep.*, 1999, **37**, 1–206.
28 D. Gross, I. Mora-Sero, T. Dittrich, A. Belaidi, C. Mauser, A. J. Houtepen, E. Da Como, A. L. Rogach and J. Feldmann, *J. Am. Chem. Soc.*, 2010, **132**, 5981–5983.
29 I. Mora-Sero, J. Bisquert, T. Dittrich, A. Belaidi, A. S. Susha and A. L. Rogach, *J. Phys. Chem. C*, 2007, **111**, 14889–14892.
30 M. Waller, T. K. Townsend, J. Zhao, E. M. Sabio, R. L. Chamousis, N. D. Browning and F. E. Osterloh, *Chem. Mater.*, 2012, **24**, 698–704.
31 F. A. Frame, T. K. Townsend, R. L. Chamousis, E. M. Sabio, T. Dittrich, N. D. Browning and F. E. Osterloh, *J. Am. Chem. Soc.*, 2011, **133**, 7264–7267.
32 A. J. Nozik, *Appl. Phys. Lett.*, 1977, **30**, 567–569.
33 R. Baba, S. Nakabayashi, A. Fujishima and K. Honda, *J. Phys. Chem.*, 1985, **89**, 1902–1905.
34 J. Greeley, T. F. Jaramillo, J. Bonde, I. B. Chorkendorff and J. K. Norskov, *Nat. Mater.*, 2006, **5**, 909–913.
35 M. H. Miles, *J. Electroanal. Chem.*, 1975, **60**, 89–96.
36 S. Trasatti, *J. Electroanal. Chem.*, 1972, **39**, 163–165.
37 S. Trasatti, *J. Electroanal. Chem.*, 1980, **111**, 125–131.
38 K. Sayama, A. Tanaka, K. Domen, K. Maruya and T. Onishi, *Catal. Lett.*, 1990, **4**, 217–222.
39 A. J. Bard and L. R. Faulkner, *Electrochemical Methods: Fundamentals and Applications*, John Wiley, New York, 2001.
40 N. Sakai, Y. Ebina, K. Takada and T. Sasaki, *J. Am. Chem. Soc.*, 2004, **126**, 5851–5858.
41 M. A. Butler and D. S. Ginley, *J. Electrochem. Soc.*, 1978, **125**, 228–232.
42 M. R. Allen, A. Thibert, E. M. Sabio, N. D. Browning, D. S. Larsen and F. E. Osterloh, *Chem. Mater.*, 2010, **22**, 1220–1228.
43 T. K. Townsend, E. M. Sabio, N. D. Browning and F. E. Osterloh, *ChemSusChem*, 2011, **4**, 185–190.
44 R. Baba and A. Fujishima, *J. Electroanal. Chem.*, 1986, **213**, 319–321.
45 J. Bera and D. Sarkar, *J. Electroceram.*, 2003, **11**, 131–137.
46 J. M. Lehn, J. P. Sauvage and R. Ziessel, *New J. Chem.*, 1980, **4**, 623–627.
47 D.-H. Chen and S.-H. Wu, *Chem. Mater.*, 2000, **12**, 1354–1360.

